

A Fast, Well-Founded Approximation to the Empirical Neural Tangent Kernel

Mohamad Amin Mohamadi
University of British Columbia
lemohama@cs.ubc.ca

Danica J. Sutherland
UBC & Amii
dsuth@cs.ubc.ca

Abstract

Empirical neural tangent kernels (eNTKs) can provide a good understanding of a given network’s representation: they are often far less expensive to compute and applicable more broadly than infinite-width NTKs. For networks with O output units (e.g. an O -class classifier), however, the eNTK on N inputs is of size $NO \times NO$, taking $\mathcal{O}((NO)^2)$ memory and up to $\mathcal{O}((NO)^3)$ computation. Most existing applications have therefore used one of a handful of approximations yielding $N \times N$ kernel matrices, saving orders of magnitude of computation, but with limited to no justification. We prove that one such approximation, which we call “sum of logits,” converges to the true eNTK at initialization for any network with a wide final “readout” layer. Our experiments demonstrate the quality of this approximation for various uses across a range of settings.

1 Introduction

The pursuit of a theoretical foundation for deep learning has lead researches to uncover interesting connections between neural Networks (NNs) and kernel methods. It has long been known that randomly initialized NNs in the infinite width limit are Gaussian processes with what is termed the NNGP kernel, and training the last layer with gradient flow under squared loss corresponds to the posterior mean (Neal, 1996; Williams, 1996; Hazan and Jaakkola, 2015; Lee et al., 2017; Matthews et al., 2018; Novak et al., 2018; Yang, 2019). Recently, Jacot et al. (2018) (building off a line of closely related prior work) showed that the same is true if we train all the parameters of the network, but using a different kernel called the Neural Tangent Kernel (NTK). Yang (2020) and Yang and Littwin (2021) later showed that this connection is architecturally universal, extending the domain from fully-connected NNs to most of the currently-used networks in practice, such as ResNets and Transformers. Lee et al. (2019) also showed that the dynamics of training wide but finite-width NNs with gradient descent can be approximated by a linear model obtained from the first-order Taylor expansion of that network around its initialization. Furthermore, they experimentally showed that this approximation approximation excellently holds even for networks that are not so wide.

In addition to theoretical insights from the results themselves, NTKs have had significant impact in diverse practical settings. Arora, Du, Li, et al. (2019) show very strong performance of NTK-based models on a variety of low-data classification and regression tasks. The condition number of an NN’s NTK has been shown correlation directly with the trainability and generalization capabilities of the NN (L. Xiao et al., 2018; L. Xiao et al., 2020); thus, Park et al. (2020) and Chen et al. (2021) have used this to develop practical algorithms for neural architecture search. Wei et al. (2022) propose generalized cross-validation to estimate the generalization ability of training a specific network, randomly initialized or pre-trained on a different dataset. Zhou et al. (2021) uses NTK regression for efficient meta-learning, and Holzmüller et al. (2022) and Wang et al. (2021) use NTKs in various ways for active learning.

There has also been significant theoretical insight gained from empirical studies of networks’ NTKs. Here are a few examples: Fort et al. (2020) uses NTK in studying the geometry of the loss landscape

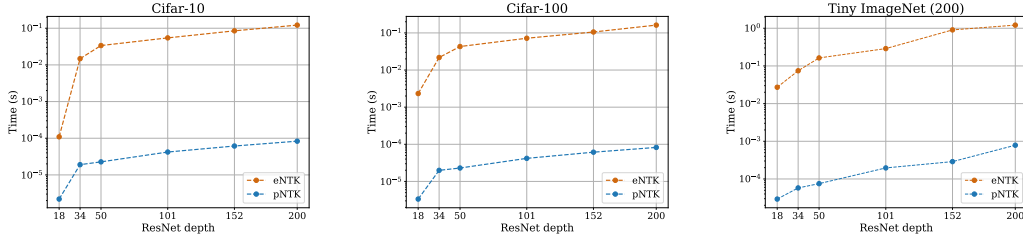


Figure 1: Comparison of **wall-clock time of evaluating the eNTK and pNTK of a pair of input datapoints** over various datasets and ResNet depths.

of the NN while evolving under gradient descent. Franceschi et al. (2021) employs NTKs to analyze the behaviour of Generative Adversarial Networks (GANs). Nguyen et al. (2020) and Nguyen et al. (2021) have used NTK to achieve excellent dataset distillation results. B. He et al. (2020) and Adlam et al. (2020) used NTKs to predict and analyze the uncertainty of a NN’s predictions. Tancik et al. (2020) uses NTKs to analyze the behaviour of MLPs in learning high frequency functions, leading to new insights into our understanding of neural radiance fields.

Given this wide array of applications, we believe NTKs will continue to be used in both theoretical and empirical aspects of deep learning.

Unfortunately, however, computing the NTK for practical networks is extremely challenging, and most of the time not even computationally feasible. The NTK of a NN is defined as the outer product of the Jacobians of the output of the NN with respect to its parameters:

$$eNTK := \Theta_{\theta}(x_1, x_2) = [J_{\theta}(f_{\theta}(x_1))] [J_{\theta}(f_{\theta}(x_2))]^{\top}, \quad (1)$$

where $J_{\theta}(f_{\theta}(x))$ denotes the Jacobian of the function f at a point x with respect to the flattened vector of all its parameters, $\theta \in \mathbb{R}^P$. Assuming $f : \mathbb{R}^D \rightarrow \mathbb{R}^O$, where D is the input dimension and O the number of outputs, we have $J_{\theta}(f_{\theta}(x)) \in \mathbb{R}^{n_L \times P}$ and $\Theta_{\theta}(x_1, x_2) \in \mathbb{R}^{O \times O}$. Thus, computing the NTK between a set of N_1 data points and a set of N_2 data points yields $N_1 N_2$ matrices each of shape $O \times O$, which we usually reshape into an $N_1 O \times N_2 O$ matrix.

When computing an eNTK on tasks involving large datasets and with multiple output neurons, e.g. in a classification model with O classes, regardless of how fast each entry is computed, the eNTK quickly becomes impractical due to its $NO \times NO$ size. For instance, the full eNTK of a classification model even on the relatively mild Cifar-10 dataset (Krizhevsky, 2009), stored in double precision, takes over 1.8 terabytes in memory. For practical usage, we need to do something better.

In this work, we present a simple trick for a strong approximation of the eNTK that removes the O^2 from the size of the kernel matrix, resulting in a factor of O^2 improvement in the memory and up to O^3 in computation. Since for typical classification datasets O is at least 10 (e.g. Cifar-10) and potentially 1 000 or more (e.g. ImageNet, Deng et al., 2009), this provides multiple orders of magnitude savings over the original NTK (1). We prove that the this approximation converges to the original NTK at a rate of $\mathcal{O}(w^{-1/2})$ for any network architecture whose final layer is fully-connected and of size $w \times O$, and the predictions of kernel regression with the approximate kernel do the same. Finally, we present diverse experimental investigations supporting our theoretical results across a range of different architectures and settings. We hope this approximation further enables researches to employ NTKs towards theoretical and empirical advances in wide networks.

Infinite NTKs In the infinite-width limit, $\hat{\Theta}_{\theta}$ converges almost surely at initialization to a particular kernel, and remains constant over the course of training. Algorithms are available to compute this expectation exactly, but they tend to be substantially more expensive than computing (1) directly for all but extremely wide networks. The convergence to this infinite-width regime is also slow in practice, and it also eliminates some of the interest of the framework: neural architecture search, predicting generalization of a pre-trained representation, and meta-learning are all considerably less interesting when we only consider infinite-width networks that do essentially no feature learning. Thus, in this paper, we focus only on the “empirical” eNTK (1).

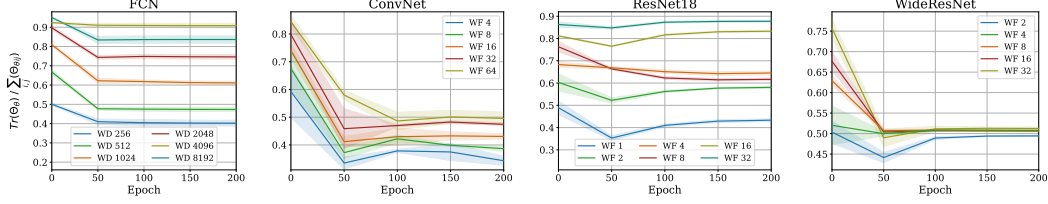


Figure 2: Evaluating the **ratio of information between on-diagonal and off-diagonal elements of Θ_θ** at initialization and throughout training, based on 1000 points from Cifar-10. The reported numbers are the average of 1000×1000 kernels each having a shape of 10×10 . The same subset has then been used to train the NN using SGD. As the NN’s width grows, the eNTK converges to being diagonal at initialization among all different architectures.

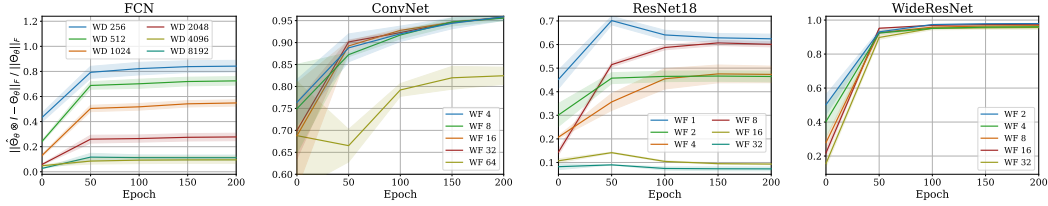


Figure 3: Evaluating the **relative difference of Frobenius norm of $\Theta_\theta(\mathcal{D}, \mathcal{D})$ and $\hat{\Theta}_\theta(\mathcal{D}, \mathcal{D}) \otimes I_O$** at initialization and throughout training, based on 1000 points from Cifar-10. As the NN’s width grows, the relative difference in $\|\Theta_\theta\|_F$ and $\|\hat{\Theta}_\theta \otimes I_O\|_F$ decreases.

2 Related Work

Among the numerous recent works that have used eNTKs either to gain insights about various phenomena in deep learning or to propose new algorithms, not many have publicized the computational costs and implementation details of computing eNTKs. Nevertheless, they’re all in agreement about the expense of such computations (Park et al., 2020; Holzmüller et al., 2022; Fort et al., 2020).

Several recent works have, mostly “secretly,” employed various techniques to avoid dealing with the full eNTK matrix; to the best of our knowledge, none provide any rigorous justifications. Wei et al. (2022, Section 2.3) point out that if the final layer of a NN is randomly initialized, the *expected* eNTK can be written as $K_0 \otimes I_C$ for some kernel K_0 , where I_O is the $O \times O$ identity matrix and \otimes is the Kronecker product. Thus, they use the approximation in which they only compute the eNTK with respect to one of the logits of the NN. Although their approach to approximating the eNTK is similar to ours, they don’t provide any rigorous bounds or empirical study of how closely the actual *eNTK* approximates its expectation in this regard. Wang et al. (2021) employs the same “single-logit” strategy, though they only mention the infinite-width limit as a motivation supporting their trick. Despite of these claims, we will see in our experiments that the eNTK is generally *not* diagonal. We will, however, prove upper bounds on distance of our approximation to the eNTK, and provide experimental support that this approximation captures the behaviour of the eNTK even when the NN’s weights are not at initialization. Park et al. (2020) and Chen et al. (2021) also seem to use a form of “single-logit” approximation to eNTK, without explicitly mentioning it. Lee et al. (2019), by contrast, do use the full eNTK, and hence never compute the kernel on more than 256 datapoints.

More recently, Novak et al. (2021) performed an in-depth analysis of computational and memory complexity required for computing the eNTK, and proposed two new approaches to reduce the time complexity of computing the eNTK in special cases (depending on the architecture of the NN) over explicitly implementing (1). We remark that as our approaches are parallel, as we propose an approximation to the eNTK and Novak et al. (2021) proposes an algorithm for computation of the eNTK, which also applies when to computing our approximation – in fact, we use their “structured derivatives” method in our experiments. Moreover, their approach does not reduce the memory complexity of computing the eNTK, typically the largest burden in practical applications.

3 Pseudo-NTK

We define the pseudo-NTK (pNTK) of the network f_θ as

$$pNTK := \hat{\Theta}_\theta(x_1, x_2) = \underbrace{\left[\nabla_\theta \left(\frac{1}{\sqrt{O}} \sum_{i=1}^O f_\theta^{(i)}(x_1) \right) \right]}_{1 \times P} \underbrace{\left[\nabla_\theta \left(\frac{1}{\sqrt{O}} \sum_{i=1}^O f_\theta^{(i)}(x_2) \right) \right]^\top}_{P \times 1}, \quad (2)$$

where $f_\theta^{(i)}(x)$ denotes the i 'th output of f_θ on the input x . Unlike eNTK which is a matrix-valued kernel for each pair of inputs, pNTK is a traditional scalar-valued kernel.

Some recent work (Arora, Du, Hu, et al., 2019; Yang, 2020; Wei et al., 2022; Wang et al., 2021) has pointed out that in the infinite width limit the NTK becomes a diagonal matrix. Thus, one can avoid computing the off-diagonal entries of the infinite-width NTK of each pair through using $\Theta_\theta(x_1, x_2) = \hat{\Theta}_\theta(x_1, x_2) \otimes I_O$, resulting in a drastic $O(O^2)$ time and memory complexity decrease.

Practitioners have accordingly used the same approach in computing the corresponding eNTK of a finite width network, but with little to no further justification. We see in our experiments that for finite width networks, the NTK is **not** diagonal. In fact, we show that for most practical networks, it is very far from being diagonal, casting doubt on the correctness of previous results that have used this scheme to calculate the NTK of a finite-width matrix. We, however, provide the first theoretical bounds of the difference between our presented approximation (2), which we call ‘‘sum of logits.’’

Before turning to the formal results and experimental evaluation, we give some intuition. First, suppose that $f_\theta^{(i)}(x) = \phi(x) \cdot v_i$, so that v_i is the i th entry of a linear read-out layer; then $\frac{1}{\sqrt{O}} \sum_{i=1}^O f_\theta^{(i)}(x) = \phi(x) \cdot \left[\frac{1}{\sqrt{O}} \sum_{i=1}^O v_i \right]$. If the vectors $v_i \sim \mathcal{N}(0, \sigma^2 I_O)$ are independent, then $\frac{1}{\sqrt{O}} \sum_{i=1}^O v_i \sim \mathcal{N}(0, \sigma^2 I_O)$ has the same distribution as any individual entry, say v_1 . Thus, at initialization, our sum of logits approximation agrees in distribution with the first-logit approximation. We prefer the sum-of-logits form for networks that are not at random initialization, however.

Calling this vector (whether the first logit or sum of logits) v , we can think of (2) as the NTK of a model with a single scalar output as a function of ϕ . When we linearize a network with that kernel for an O -class classification problem, getting the formula (6) discussed in Section 4.3, we end up, effectively, with a one-vs-rest classifier scheme. Thus, we can think of the pseudo-NTK as approximating the process of training O one-vs-rest classifiers, rather than a single O -way classifier.

4 Approximation Quality of Pseudo-NTK

We will now study various aspects of the approximation of (2) to (1), both in theory and empirically. To experimentally evaluate our claims, we present various experiments that compare the targeted characteristic of pNTK vs eNTK both at initialization and throughout training. We present our experiments on four mostly-used architectures, namely, fully-connected networks (FCN) of depth 3 (as in Lee et al., 2019; Lee et al., 2020), fully-convolutional networks (ConvNet) of depth 8 (as in Arora, Du, Hu, et al., 2019; Arora, Du, Li, et al., 2019; Lee et al., 2020), ResNet18 (K. He et al., 2016) and WideResNet-16- k (Zagoruyko and Komodakis, 2016). For each architecture, we test our measurements on different widths, as mentioned in the plot legends: for FCN, we show exact widths, while for others we show a widening factor (details in Appendix A). For consistency, we use data from the Cifar-10 dataset. Each experiment is repeated using three seeds, and the corresponding error bars are plotted. When bars are not present, it is because they interfered with clear interpretation of the plots, but versions with error bars are all available in the appendix.

Each network on each experiment is trained for 200 epochs using mini-batch stochastic gradient descent (SGD), run on NVIDIA V100 GPUs with 32GB of memory. Details on the batch sizes and learning rates used for each NN can be found in Appendix A. The measured statistic for each experiment has been reported at five different epochs, namely, 0, 50, 100, 150, 200.

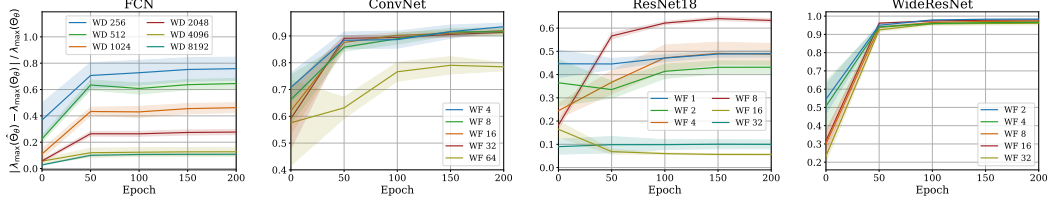


Figure 4: Evaluating the **relative difference of λ_{\max} of $\Theta_{\theta}(\mathcal{D}, \mathcal{D})$ and $\hat{\Theta}_{\theta}(\mathcal{D}, \mathcal{D})$** at initialization and throughout training. The kernels have been evaluated using a subset ($|\mathcal{D}| = 1000$) of points from Cifar-10. As the NN’s width grows, the relative difference in $\lambda_{\max}(\Theta_{\theta}(\mathcal{D}, \mathcal{D}))$ and $\lambda_{\max}(\hat{\Theta}_{\theta}(\mathcal{D}, \mathcal{D}))$ decreases.

4.1 Pseudo-NTK converges to eNTK as the final layer’s width grows

The first crucial thing to verify is whether the pNTK kernel matrix approximates the true eNTK as a whole. We study this first in terms of Frobenius norm.

Theorem 1 (Informal). *Let $f_{\theta} : \mathbb{R}^D \rightarrow \mathbb{R}^O$ be a NN with a final dense read-out layer of width w . Let $\hat{\Theta}_{\theta}(x_1, x_2)$ be the corresponding pNTK of f_{θ} as in Equation (2) and $\Theta_{\theta}(x_1, x_2)$ the corresponding eNTK as in Equation (1). When the final read-out layer is properly initialized, with high probability,*

$$\left\| \frac{1}{\sqrt{w}} \hat{\Theta}_{\theta}(x_1, x_2) \otimes I_O - \frac{1}{\sqrt{w}} \Theta_{\theta}(x_1, x_2) \right\|_F \in \mathcal{O}(w^{-\frac{1}{2}}). \quad (3)$$

Remark 2. *This behaviour is architecturally universal. The network can be of any architecture at all, as long as it has a densely-connected final output layer with w inputs.*

Remark 3. *For this approximation to hold, only the last layer’s weights need to be distributed according to the so-called NTK parameterization (Lee et al., 2019; Yang, 2020; Arora, Du, Hu, et al., 2019). Thus, the approximation equally applies to networks with pre-trained weights (other than in the read-out layer), e.g. in transfer learning as studied by Wei et al. (2022).*

Remark 4. *In most use-cases, a kernel can be replaced with a scaled version of the same kernel without any side effects. For instance, in kernel regression without regularization (as used in many applications of NTKs) or analysis of eigen-spectrum of the gram-matrix of a kernel, scaling the kernel by a real value does not change any factor in the analysis.*

Theorem 1 provides the first upper bound on the convergence rate of pNTK towards eNTK. A formal statement for Theorem 1 and its proof are in Appendix B.2.

Experimental results in Figure 2 support the fact that as width grows, the ratio between off-diagonal and diagonal elements of $\Theta_{\theta}(x_1, x_2)$ converges to zero. Furthermore, Figure 3 provides experimental support that as width grows, $\hat{\Theta}_{\theta} \otimes I_O$ converges to Θ_{θ} in terms of relative Frobenius norm.

However, as it can be seen in the figures, these results don’t necessarily apply to the NNs whose readout layers are not at initialization (i.e., after a few epochs of training). This naturally gives rise to the question: *Can the pNTK be used to analyze and represent NNs whose parameters are far from initialization?* In what comes next, we dive deeper into experimentally figuring out the answer to this question from various aspects.

4.2 Pseudo-NTK’s eigenspectrum converges to eNTK’s eigenspectrum as width grows

As discussed before, the conditioning of a network’s eNTK has been shown to be closely related to generalization properties of the network, such as trainability and generalization risk (L. Xiao et al., 2018; L. Xiao et al., 2020; Wei et al., 2022). Thus, we would like to know how well the pNTK’s eigenspectrum approximates that of the eNTK. The following proposition gives a partial result.

Theorem 5 (Informal). *Let $f_{\theta} : \mathbb{R}^D \rightarrow \mathbb{R}^O$ be a NN with a final dense read-out layer of width w . Let $\hat{\Theta}_{\theta}(x_1, x_2)$ be the corresponding pNTK of f_{θ} as in Equation (2) and $\Theta_{\theta}(x_1, x_2)$ the corresponding eNTK as in Equation (1). When the final read-out layer is properly initialized, with high probability,*

$$\lambda_{\max} \left(\frac{1}{\sqrt{w}} \hat{\Theta}_{\theta}(x_1, x_2) \otimes I_O \right) - \lambda_{\max} \left(\frac{1}{\sqrt{w}} \Theta_{\theta}(x_1, x_2) \right) \in \mathcal{O}(w^{-\frac{1}{2}}). \quad (4)$$

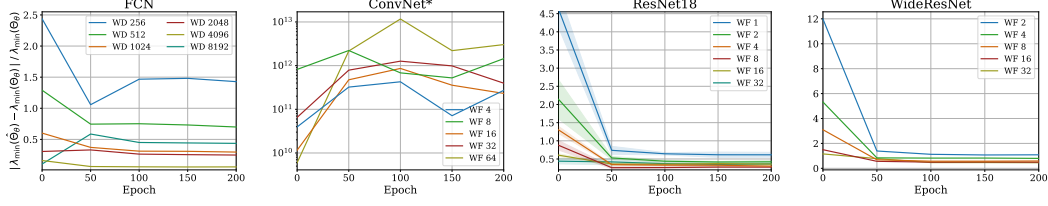


Figure 5: Evaluating the **relative difference of λ_{\min} of $\Theta_\theta(\mathcal{D}, \mathcal{D})$ and $\hat{\Theta}_\theta(\mathcal{D}, \mathcal{D})$** at initialization and throughout training. The kernels have been evaluated using a subset ($|\mathcal{D}| = 1000$) of points from Cifar-10. As the NN’s width grows, the relative difference in $\lambda_{\min}(\Theta_\theta(\mathcal{D}, \mathcal{D}))$ and $\lambda_{\min}(\hat{\Theta}_\theta(\mathcal{D}, \mathcal{D}))$ decreases. Note the extremely large values reported for ConvNet. As observed previously in Lee et al. (2020) and L. Xiao et al. (2020), CNN-GAP is ill-conditioned and $\lambda_{\min}(\Theta_\theta(\mathcal{D}, \mathcal{D})) \rightarrow 0$, while $\lambda_{\min}(\hat{\Theta}_\theta(\mathcal{D}, \mathcal{D})) > 0.001$, causing the huge discrepancy. More details in Appendix B.3.

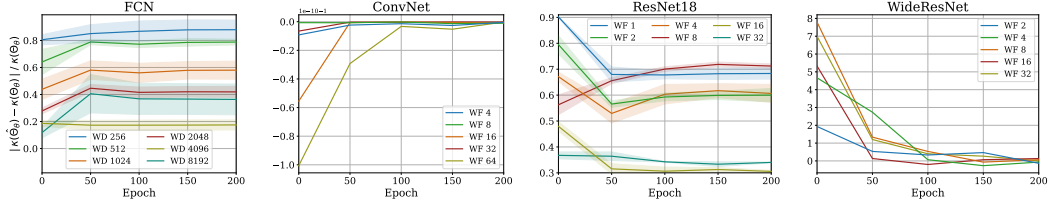


Figure 6: Evaluating the **relative difference of condition number of eNTK and pNTK** at initialization and throughout training. Condition number is defined as $\kappa(K) = \lambda_{\max}(K) / \lambda_{\min}(K)$. The kernels have been evaluated using a subset ($|\mathcal{D}| = 1000$) of points from Cifar-10. As the NN’s width grows, the relative difference in $\lambda_{\min}(\Theta_\theta(\mathcal{D}, \mathcal{D}))$ and $\lambda_{\min}(\hat{\Theta}_\theta(\mathcal{D}, \mathcal{D}))$ decreases. The bizarre values found in the ConvNet plot can be addressed as discussed in Figure 5; more details in Appendix B.3.

Theorem 5 provides an upper bound on the difference between the maximum eigenvalue of pNTK versus the maximum eigenvalue of eNTK based on the NN’s last layer’s width. A formal statement for Theorem 5 and its proof are given in Appendix B.3. Experimental results in Figure 4 support the fact that as width grows, the max eigenvalue of Θ_θ converge to the max eigenvalue of $\hat{\Theta}_\theta$. Figure 5 provides similar experimental support regarding the minimum eigenvalues of $\hat{\Theta}_\theta$ and Θ_θ in terms of relative difference. Together, these two results intuitively imply that the condition number $\kappa(K) = \lambda_{\max}(K) / \lambda_{\min}(K)$ should become similar as width grows; this is also supported by results in Figure 6. However, as in the previous subsection, these results don’t necessarily apply to the NNs whose last layer parameters are not at initialization (i.e., after a few epochs of training).

Interestingly, the rate of increase/decrease in the difference between maximum and minimum eigenvalues and the condition numbers between pNTK and eNTK do not have necessarily have a monotonic behaviour. We show the exact values of λ_{\min} , λ_{\max} and κ for different architectures, widths at initialization and throughout training in Appendix B.3. Specifically, we observe that in ConvNet, WideResNet and ResNet18 architectures, λ_{\min} is close to zero at initialization, but grows during training; the inverse phenomenon is observed with FCNs. Further investigations of these statistics might reveal interesting insights about the behaviour of NNs trained with SGD.

4.3 Kernel regression using pNTK vs Kernel regression using eNTK

Lee et al. (2019) proved that as a finite NN’s width grows, its training dynamics can be well approximated using the first-order Taylor expansion of that NN around its initialization (a *linearized neural network*). Informally, they showed that when f is wide enough, its predictions after being trained using gradient descent with suitably small learning rate on the training set \mathcal{D} can be approximated by those of the linearized network f^{lin} :

$$\underbrace{f^{\text{lin}}(x)}_{1O \times 1} = \underbrace{f_0(x)}_{1O \times 1} + \underbrace{\Theta_0(x, \mathcal{D})}_{1O \times NO} \underbrace{\Theta_0(\mathcal{D}, \mathcal{D})^{-1}}_{NO \times NO} \underbrace{(\mathcal{Y}_{\mathcal{D}} - f_0(\mathcal{D}))}_{NO \times 1}, \quad (5)$$

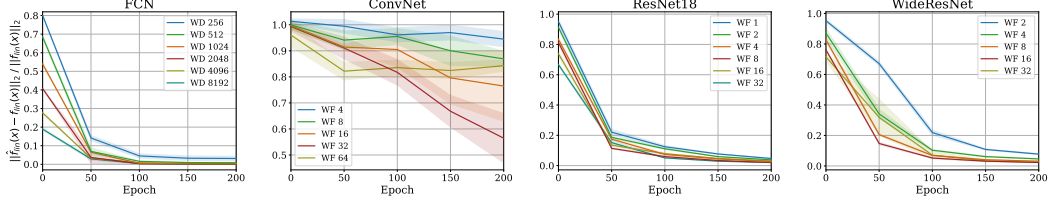


Figure 7: Evaluating the **relative norm difference of kernel regression outputs using eNTK and pNTK as in Equation (5) and Equation (6)** at initialization and throughout training. The kernel regression has been done on $|\mathcal{D}| = 1000$ training points and $|\mathcal{X}| = 500$ test points randomly selected from Cifar-10’s train and test sets. As the NN’s width grows, the relative difference in $\hat{f}^{lin}(\mathcal{X})$ and $f^{lin}(\mathcal{X})$ decreases at initialization. Surprisingly, the difference between these two continues to quickly vanish throughout the training process using SGD.

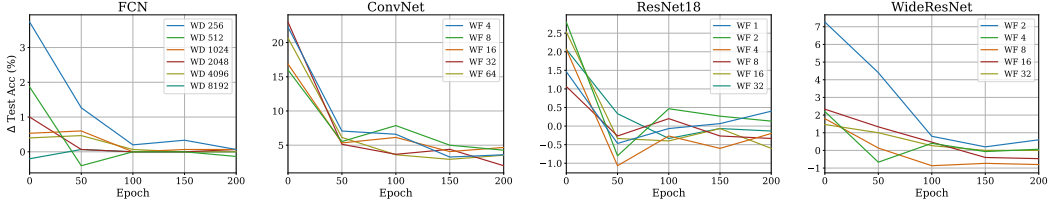


Figure 8: Evaluating the **accuracy difference of kernel regression outputs using eNTK and pNTK as in Equation (5) and Equation (6)** at initialization and throughout training. **Kernel regression using pNTK always achieves a higher test accuracy in comparison to kernel regression using eNTK.** The kernel regression has been done on $|\mathcal{D}| = 1000$ training points and $|\mathcal{X}| = 500$ test points randomly selected from Cifar-10’s train and test sets. As the NN’s width grows, the prediction accuracy of in \hat{f}^{lin} and f^{lin} decreases at initialization. Again, the difference between these two continues to vanish throughout the training process using SGD.

where $\mathcal{Y}_{\mathcal{D}}$ is the matrix of one-hot labels for the training points \mathcal{D} , and Θ_0 is the eNTK of f at initialization f_0 . This is simply kernel regression on the training data \mathcal{D} using the kernel Θ_0 and prior mean f_0 . Wei et al. (2022) use the same kernel in a generalized cross-validation estimator (Craven and Wahba, 1978) to predict the generalization risk of the NN. As discussed before, using the eNTK in these applications is practically infeasible, due to huge time and memory complexity of the kernel, but we show the pNTK approximates $f^{lin}(x)$ with much improved time and memory complexity.

Theorem 6 (Informal). Let $f_\theta : \mathbb{R}^D \rightarrow \mathbb{R}^O$ be a NN with a final dense read-out layer of width w . Let $\hat{\Theta}_\theta(x_1, x_2)$ be the pNTK of f_θ as in (2), and $\Theta_\theta(x_1, x_2)$ its eNTK as in (1). Define

$$\underbrace{\hat{f}^{lin}(x)}_{1 \times O} := \underbrace{f_0(x)}_{1 \times O} + \underbrace{\hat{\Theta}_\theta(x, \mathcal{D})}_{1 \times N} \underbrace{\hat{\Theta}_\theta(\mathcal{D}, \mathcal{D})^{-1}}_{N \times N} \underbrace{(\mathcal{Y}_{\mathcal{D}} - f_0(\mathcal{D}))}_{N \times O}. \quad (6)$$

With proper reshaping, when the final read-out layer is properly initialized, with high probability,

$$\|\hat{f}^{lin}(x) - f^{lin}(x)\| \in \mathcal{O}(w^{-\frac{1}{2}}). \quad (7)$$

Theorem 6 provides an upper bound on the norm difference of \hat{f}^{lin} from (6) and f^{lin} from Equation (5) based on the NN’s last layer’s width. A formal statement is given and proved in Appendix B.4.

Experimental results in Figure 7 show that as width grows, the predictions of kernel regression using $\hat{\Theta}_\theta$ converge to the prediction of those obtained from using Θ_θ , while requiring orders of magnitude of less memory and time to compute. Figure 8 shows similar results for the difference in prediction accuracies achieved using kernel regression through $\hat{\Theta}_\theta$ and Θ_θ kernels. Appendix B.4 also shows the values of the prediction accuracies, as well as further analysis of how well the *linearized network* predicts the final accuracy of the trained model for each architecture and width pair. Although $\|\hat{f}^{lin}(x) - f^{lin}(x)\|_2$ decreases with width of the network in Figure 7 at initialization, this does not necessarily translate to a monotonic behaviour in prediction accuracies, a non-smooth function of the vector of predictions; we do see that the expected pattern more or less holds, however.

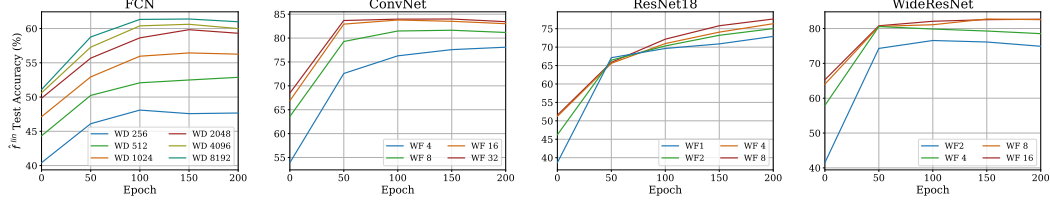


Figure 9: Evaluating the **test accuracy of kernel regression predictions using pNTK as in Equation (6) on the full Cifar-10 dataset** at initialization and throughout training. As the NN’s width grows, the test accuracy of \hat{f}^{lin} is also improved, but eventually saturates with the growing width. Using trained weights in computation of pNTK results in improved test accuracy of \hat{f}^{lin} .

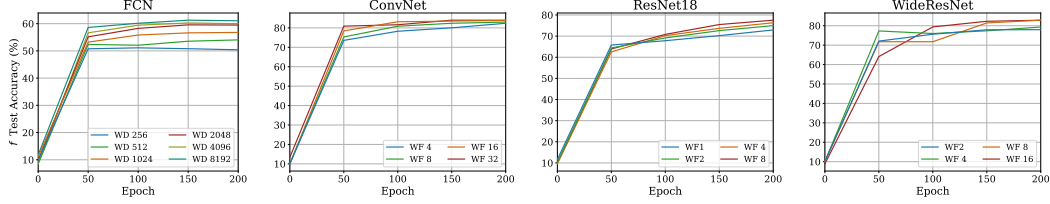


Figure 10: Evaluating the **test accuracy of model f throughout SGD training on the full Cifar-10 dataset**. In contrast to \hat{f}^{lin} , the test accuracy of f does not significantly improve with growing width.

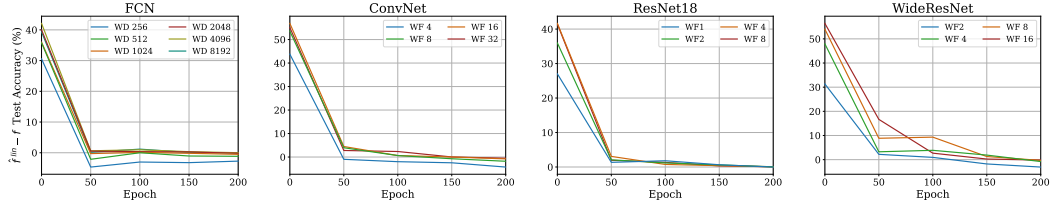


Figure 11: Evaluating the **difference in test accuracy of kernel regression using pNTK as in (6) vs the current model f throughout SGD training on the full Cifar-10 dataset**: how much does the result of linearization with the current representation \hat{f}^{lin} improve prediction accuracy over SGD at this point?

A surprising outcome depicted in Figures 7 and 8 is that while training the model’s parameters, predictions of \hat{f}^{lin} and f^{lin} converge very quickly. This is particularly intriguing as it’s in contrast with the experimental results depicted in Figures 2 to 4 and 6. In other words, although the kernels Θ_θ and $\hat{\Theta}_\theta \otimes I_O$ seem to be diverging in Frobenius norm, eigenspectrum, and so on, kernel regression using those two kernels converges quickly, so that after 50 epochs the difference in predictions almost totally vanishes. We believe further investigation of why this phenomenon is observed could lead to new interesting insights about the training dynamics of NNs.

5 Kernel Regression using pNTK on full Cifar-10 dataset

Thanks to the reduction in time and memory complexity of pNTK over eNTK, motivated by Theorem 6 and experimental findings in Figure 8, we finally evaluate the corresponding pNTKs of the four architectures that we have used in our experimental evaluations in different widths using full Cifar-10 data, at initialization and throughout training the models under SGD. As mentioned previously, running kernel regression with eNTK on all of Cifar-10 would require evaluating 25×10^{10} Jacobian-vector products and more than ≈ 1.8 terabytes of memory; using pNTK, this can be done with a far more reasonable 25×10^8 Jacobian-vector products and ≈ 18 gigabytes of memory. This is still a heavy load compared to, say, direct SGD training, but is within the reach of standard compute nodes.

Figure 9 shows the test accuracy of \hat{f}^{lin} on the full train and test sets of Cifar-10. Theoretically, in the infinite-width limit, the test accuracy of \hat{f}^{lin} at initialization (and later, because the kernel stays constant in this regime) and the final test accuracy of f should be the same: that is, the epoch 0 points in Figure 9 would agree with the roughly the epoch 200 points in Figure 10. This comparison is plotted directly in Appendix C.

Furthermore, the test accuracies of predictions of kernel regression using the pNTK are lower than those achieved by the NTKs of infinite-width counterparts for fully-connected and fully-convolution networks. This is consistent with results on eNTK by Arora, Du, Hu, et al. (2019) and Lee et al. (2020), although Arora, Du, Hu, et al. (2019) studied only a “Cifar-2” version.

It is worth noting from Figures 9 and 11 that, in contrast to the findings of Fort et al. (2020), we observe that the corresponding pNTK of the NN f continues to change even after epoch 50 of SGD training. Although for fully-connected networks and some versions of ResNet18 this change is not significant, in fully-convolutional networks and WideResNets the pNTK continues to exhibit changes until epoch 150, where the training error has vanished. We remark that Fort et al. (2020) analyzed eNTKs based on only 500 random samples from Cifar-10, while the pNTK approximation has enabled us to run our analysis on the $100\times$ larger full dataset.

Lastly, to help the community better analyze the properties of NNs and their training dynamics and avoid wasting computation by redoing this work, we plan to share computed pNTKs for all the mentioned architectures and widths, as well as pNTKs of ResNets with 34, 50, 101, 152 and 200 layers on Cifar-10, Cifar-100 and Fashion-MNIST (H. Xiao et al. (2017)) datasets, both at initialization and using pretrained ImageNet (Deng et al., 2009) weights. We hope that our contribution will enable further analyses and breakthroughs towards a stronger theoretical understanding of the training dynamics of deep neural networks.

6 Limitations and Discussion

One major limitation of this work is that we were not able to theoretically analyze what happens to the pNTK or eNTK during SGD training of the network. In particular, the fast convergence of \hat{f}^{lin} and f^{lin} when training the network, as seen in Figures 7 and 8, runs counter to our expectations based on the approximation worsening in Frobenius norm (Figure 7), maximum eigenvalue (Figure 4), and condition number (Figure 6). This seems likely to be very important to practical use of the pNTK.

Perhaps relatedly, we were also not able to rigorously determine why pNTK consistently results in higher prediction accuracies than when kernel regression is done using eNTK, given that our motivation for pNTK is entirely in terms of approximating the eNTK (Figure 8). Intuitively, this may be related to a regularization-type effect: the pNTK corresponds to a particularly limited choice of a “separable” operator-valued kernel (e.g. Álvarez et al., 2012). Separable kernels are a common choice in that literature for both computational and regularization reasons; by enforcing this particularly simple form, we remove many degrees of freedom relating to the interaction between “tasks” (different classes) that may be unnecessary or hard to estimate accurately with the eNTK. This might, in some sense, correspond to a one-vs-one rather than one-vs-rest framework in the intuitive sense discussed in Section 3. But understanding this question in more detail might require a more detailed understanding of the structure of the eNTK at finite width, and/or a much more detailed understanding of the interaction between classes in the dataset with learning in the NTK regime.

Another limitation is that even the pNTK is still rather expensive to compute compared to running SGD on neural networks. It might make for a better starting point than the full eNTK for other speedup methods, however, like kernel approximation schemes or advanced linear algebra solvers (e.g. Rudi et al., 2017).

Overall, our pseudo-NTK approach to approximating the empirical Neural Tangent Kernel has provable bounds, good empirical performance, and multiple orders of magnitude improvement in runtime and speed over the direct empirical NTK. We evaluate our claims and the quality of the approximation under diverse settings, giving new insights into the behaviour of the empirical NTK with trained representations. We help justify the correctness of recent approximation schemes, and hope that our rigorous results and thorough experimentation will help researchers develop a deeper understanding of the training dynamics of finite networks, and develop new practical applications of the NTK theory.

Acknowledgments and Disclosure of Funding

We would like to thank Roman Novak and Wonho Bae for productive discussions. We would also like to thank Roman Baranowski for helping us with our computational requirements. This research was enabled in part by support, computational resources, and services provided by the Canada CIFAR AI Chairs program, Advanced Research Computing at the University of British Columbia, WestGrid, Calcul Québec, and the Digital Research Alliance of Canada.

References

- Adlam, Ben, Jaehoon Lee, Lechao Xiao, Jeffrey Pennington, and Jasper Snoek (2020). “Exploring the Uncertainty Properties of Neural Networks’ Implicit Priors in the Infinite-Width Limit.” arXiv: [2010.07355](#).
- Álvarez, Mauricio A., Lorenzo Rosasco, and Neil D. Lawrence (2012). “Kernels for Vector-Valued Functions: A Review.” *Foundations and Trends® in Machine Learning* 4.3, pp. 195–266. DOI: [10.1561/22000000036](#). arXiv: [1106.6251](#).
- Arora, Sanjeev, Simon S Du, Wei Hu, Zhiyuan Li, Ruslan Salakhutdinov, and Ruosong Wang (2019). “On Exact Computation with an Infinitely Wide Neural Net.” *NeurIPS*.
- Arora, Sanjeev, Simon S Du, Zhiyuan Li, Ruslan Salakhutdinov, Ruosong Wang, and Dingli Yu (2019). “Harnessing the power of infinitely wide deep nets on small-data tasks.” arXiv: [1910.01663](#).
- Chen, Xiangning, Cho-Jui Hsieh, and Boqing Gong (2021). “When vision transformers outperform ResNets without pre-training or strong data augmentations.” arXiv: [2106.01548](#).
- Craven, Peter and Grace Wahba (1978). “Smoothing noisy data with spline functions.” *Numerische mathematik* 31.4, pp. 377–403.
- Deng, Jia, Wei Dong, Richard Socher, Li-Jia Li, Kai Li, and Li Fei-Fei (2009). “Imagenet: A large-scale hierarchical image database.” *2009 IEEE conference on computer vision and pattern recognition*. Ieee, pp. 248–255.
- Fort, Stanislav, Gintare Karolina Dziugaite, Mansheej Paul, Sepideh Kharaghani, Daniel M Roy, and Surya Ganguli (2020). “Deep learning versus kernel learning: an empirical study of loss landscape geometry and the time evolution of the neural tangent kernel.” *Advances in Neural Information Processing Systems* 33, pp. 5850–5861.
- Franceschi, Jean-Yves, Emmanuel de Bézenac, Ibrahim Ayed, Mickaël Chen, Sylvain Lamprier, and Patrick Gallinari (2021). “A neural tangent kernel perspective of gans.” arXiv: [2106.05566](#).
- Hazan, Tamir and Tommi Jaakkola (2015). “Steps toward deep kernel methods from infinite neural networks.” arXiv: [1508.05133](#).
- He, Bobby, Balaji Lakshminarayanan, and Yee Whye Teh (2020). “Bayesian deep ensembles via the neural tangent kernel.” *Advances in Neural Information Processing Systems* 33, pp. 1010–1022.
- He, Kaiming, Xiangyu Zhang, Shaoqing Ren, and Jian Sun (2016). “Deep residual learning for image recognition.” *Proceedings of the IEEE conference on computer vision and pattern recognition*, pp. 770–778.
- Holzmüller, David, Viktor Zaverkin, Johannes Kästner, and Ingo Steinwart (2022). “A Framework and Benchmark for Deep Batch Active Learning for Regression.” arXiv: [2203.09410](#).
- Jacot, Arthur, Franck Gabriel, and Clément Hongler (2018). “Neural Tangent Kernel: Convergence and Generalization in Neural Networks.” *NeurIPS*.
- Krizhevsky, Alex (2009). “Learning Multiple Layers of Features from Tiny Images.”
- Lee, Jaehoon, Yasaman Bahri, Roman Novak, Samuel S Schoenholz, Jeffrey Pennington, and Jascha Sohl-Dickstein (2017). “Deep neural networks as gaussian processes.” arXiv: [1711.00165](#).
- Lee, Jaehoon, Samuel Schoenholz, Jeffrey Pennington, Ben Adlam, Lechao Xiao, Roman Novak, and Jascha Sohl-Dickstein (2020). “Finite versus infinite neural networks: an empirical study.” *Advances in Neural Information Processing Systems* 33, pp. 15156–15172.
- Lee, Jaehoon, Lechao Xiao, Samuel Schoenholz, Yasaman Bahri, Roman Novak, Jascha Sohl-Dickstein, and Jeffrey Pennington (2019). “Wide Neural Networks of Any Depth Evolve as Linear Models Under Gradient Descent.” *NeurIPS*.
- Matthews, Alexander G de G, Mark Rowland, Jiri Hron, Richard E Turner, and Zoubin Ghahramani (2018). “Gaussian process behaviour in wide deep neural networks.” arXiv: [1804.11271](#).
- Neal, Radford M (1996). “Priors for infinite networks.” *Bayesian Learning for Neural Networks*. Springer, pp. 29–53.
- Nguyen, Timothy, Zhourong Chen, and Jaehoon Lee (2020). “Dataset meta-learning from kernel ridge-regression.” arXiv: [2011.00050](#).

- Nguyen, Timothy, Roman Novak, Lechao Xiao, and Jaehoon Lee (2021). “Dataset distillation with infinitely wide convolutional networks.” *Advances in Neural Information Processing Systems* 34.
- Novak, Roman, Jascha Sohl-Dickstein, and Samuel Stern Schoenholz (2021). “Fast Finite Width Neural Tangent Kernel.” *Fourth Symposium on Advances in Approximate Bayesian Inference*.
- Novak, Roman, Lechao Xiao, Jaehoon Lee, Yasaman Bahri, Greg Yang, Jiri Hron, Daniel A Abolafia, Jeffrey Pennington, and Jascha Sohl-Dickstein (2018). “Bayesian deep convolutional networks with many channels are gaussian processes.” arXiv: [1810.05148](#).
- Park, Daniel S, Jaehoon Lee, Daiyi Peng, Yuan Cao, and Jascha Sohl-Dickstein (2020). “Towards nngp-guided neural architecture search.” arXiv: [2011.06006](#).
- Rudi, Alessandro, Luigi Carratino, and Lorenzo Rosasco (2017). “FALKON: An Optimal Large Scale Kernel Method.” *NeurIPS*. arXiv: [1705.10958](#).
- Tancik, Matthew, Pratul Srinivasan, Ben Mildenhall, Sara Fridovich-Keil, Nithin Raghavan, Utkarsh Singhal, Ravi Ramamoorthi, Jonathan Barron, and Ren Ng (2020). “Fourier features let networks learn high frequency functions in low dimensional domains.” *Advances in Neural Information Processing Systems* 33, pp. 7537–7547.
- Wainwright, Martin J. (2019). *High-Dimensional Statistics: A Non-Asymptotic Viewpoint*. Cambridge Series in Statistical and Probabilistic Mathematics. Cambridge University Press. DOI: [10.1017/9781108627771](#).
- Wang, Haonan, Wei Huang, Andrew Margenot, Hanghang Tong, and Jingrui He (2021). “Deep Active Learning by Leveraging Training Dynamics.” arXiv: [2110.08611](#).
- Wei, Alexander, Wei Hu, and Jacob Steinhardt (2022). “More Than a Toy: Random Matrix Models Predict How Real-World Neural Representations Generalize.” arXiv: [2203.06176](#).
- Williams, Christopher (1996). “Computing with infinite networks.” *Advances in neural information processing systems* 9.
- Xiao, Han, Kashif Rasul, and Roland Vollgraf (2017). “Fashion-mnist: a novel image dataset for benchmarking machine learning algorithms.” *arXiv preprint arXiv:1708.07747*.
- Xiao, Lechao, Yasaman Bahri, Jascha Sohl-Dickstein, Samuel Schoenholz, and Jeffrey Pennington (2018). “Dynamical isometry and a mean field theory of cnns: How to train 10,000-layer vanilla convolutional neural networks.” *International Conference on Machine Learning*. PMLR, pp. 5393–5402.
- Xiao, Lechao, Jeffrey Pennington, and Samuel Schoenholz (2020). “Disentangling trainability and generalization in deep neural networks.” *International Conference on Machine Learning*. PMLR, pp. 10462–10472.
- Yang, Greg (2019). “Wide feedforward or recurrent neural networks of any architecture are gaussian processes.” *Advances in Neural Information Processing Systems* 32.
- (2020). *Tensor Programs II: Neural Tangent Kernel for Any Architecture*. arXiv: [2006.14548 \[stat.ML\]](#).
- Yang, Greg and Etai Littwin (2021). *Tensor Programs IIb: Architectural Universality of Neural Tangent Kernel Training Dynamics*. arXiv: [2105.03703 \[cs.LG\]](#).
- Zagoruyko, Sergey and Nikos Komodakis (2016). “Wide Residual Networks.” *BMVC*.
- Zhou, Yufan, Zhenyi Wang, Jiayi Xian, Changyou Chen, and Jinhui Xu (2021). “Meta-learning with neural tangent kernels.” arXiv: [2102.03909](#).

A Details of experimental setup

In this section, we present the details on the experimental setup used for the plots depicted in the main body of the paper. As mentioned, the exact width for FCNs have been reported. For WideResNet-16-k we use two block layers, and the initial convolution in the network has a width of $16WF$ where WF is the reported WF . For instance, $WF = 16$ means that the first block layer has a width of 256 and the second block layer has a width of 512. For ResNet18, we also used the same approach, multiplying WF by 16. Thus, when $WF = 4$, the constructed network will have the exact architecture as the classical ResNet18 architecture reported. A WF of 16 means a ResNet18 with each layer being 4 times wider than the original width.

When training the neural networks using SGD, a constant batch size of 128 was used across all different networks and different dataset sizes used for training. The learning rate for all networks was also fixed to 0.1. However, not all networks were trainable with this fixed learning rate, as the gradients would sometimes blow up and give NaN training loss, typically for the largest width of each mentioned architecture. In those cases, we decreased the learning rate to 0.01 to train the networks.

Note that to be consistent with the literature on NTKs techniques like Data Augmentation have been turned off but a weight decay of 0.0001 along with a momentum of 0.9 for SGD is used. Data Augmentation here plays an important role in the attained test accuracies of the fully trained networks.

B Further results on the approximation quality

In this section we'll lay out the proofs of the theorems provided in the main text, mainly Theorems 1, 5 and 6. Towards this, we first define some notation. Consider a NN $f : \mathbb{R}^D \rightarrow \mathbb{R}^O$. We assume the final read-out layer of the NN f is a dense layer with width w . Assuming the NN f has L layers, we define θ_l to be the corresponding parameters of layer $l \in \{1, 2, \dots, L\}$. Furthermore, let's define $g : \mathbb{R}^O \rightarrow \mathbb{R}^w$ as the output of the immediate last layer of the NN f , such that $f(x) = \theta_L g(x)$ for some $\theta_L \in \mathbb{R}^{O \times w}$. Finally, we assume that the last layer is distributed according to the so-called "NTK parameterization", meaning that $W_{i,j} \sim \frac{\sigma_L}{\sqrt{w}} z$ for some $\sigma_L \in \mathbb{R}^+$ where $z \sim \mathcal{N}(0, 1)$. We remark that all our results in this section follow the notation and assumptions mentioned in this paragraph.

As shown by Lee et al. (2019) and Yang (2020), the NTK can be reformulated as the layer-wise sum of gradients (when the parameters of each layer θ_l are assumed to be vectorized) of the output with respect to θ_l . Accordingly, we denote eNTK of a NN f as

$$\Theta_f(x_1, x_2) = \sum_{l=1}^L \nabla_{\theta_l} f(x_1) \nabla_{\theta_l} f(x_2)^\top. \quad (8)$$

Now, noting that as the final layer of f is a dense layer, we can use the chain rule to write $\nabla_{\theta_l} f(x)$ as $\frac{\partial f}{\partial g(x)} \frac{\partial g(x)}{\partial \theta_l}$ where $\frac{\partial f(x)}{\partial g(x)} = \theta_L$. Thus, we can rewrite (8) as

$$\begin{aligned} \Theta_f(x_1, x_2) &= \sum_{l=1}^{L-1} \theta_L \nabla_{\theta_l} g(x_1) \nabla_{\theta_l} g(x_2)^\top \theta_L^\top + \nabla_{\theta_L} f(x_1) \nabla_{\theta_L} f(x_2)^\top \\ &= \theta_L \left(\sum_{l=1}^{L-1} \nabla_{\theta_l} g(x_1) \nabla_{\theta_l} g(x_2)^\top \right) \theta_L^\top + g(x_1)^\top g(x_2) I_O \\ &= \theta_L \Theta_g(x_1, x_2) \theta_L^\top + g(x_1)^\top g(x_2) I_O. \end{aligned} \quad (9)$$

Applying Equation (9), we can already see that the pNTK of a network f simply calculates a weighted summation of all elements of eNTK into a scalar, since it can be seen as adding a new final dense layer to the network f with the fixed weight vector $\frac{1}{\sqrt{O}} \mathbf{1}_O$ where $\mathbf{1}_O$ is the O -dimensional vector consisting of all 1s.

Before moving on with the approximation proofs, we would like to mention that the proofs in this section rely heavily on concentration inequalities of *sub-exponential* random variables. Thus, we start by providing some background about sub-exponential random variables and the related concentration inequalities that we will use later on.

B.1 Background on Sub-Exponential random variables

A random variable X with mean μ is called *sub-exponential* (Wainwright, 2019) if there are non-negative parameters (ν, α) such that

$$\mathbb{E}[e^{\lambda(X-\mu)}] \leq e^{\frac{\nu^2 \lambda^2}{2}} \quad \text{for all } |\lambda| < \frac{1}{\alpha}.$$

We denote $X \sim SE(\nu, \alpha)$ to show that X is a sub-exponential random variable with parameters (ν, α) .

A famous sub-exponential random variable is the product of two standard normal distributions such that the two factors are independent ($X_1 = z_1 z_2 \sim SE(\sqrt{2}, \sqrt{2})$) or the same ($X_2 = z^2 \sim SE(2, 4)$) where $z \sim \mathcal{N}(0, 1)$. We now present a few lemmas regarding sub-exponential random variables that will come in handy in the later subsections of the appendix.

Lemma 7. *If a random variable X is sub-exponential with parameters (ν, α) , then the random variable sX where $s \in \mathbb{R}^+$ is also sub-exponential with parameters $(s\nu, s\alpha)$.*

Proof. Consider $X \sim SE(\nu, \alpha)$ and $X' = sX$ with $\mathbb{E}[X'] = s \mathbb{E}[X]$, then according to the definition of a sub-exponential random variable

$$\begin{aligned} \mathbb{E}[\exp(\lambda(X - \mu))] &\leq \exp\left(\frac{\nu^2 \lambda^2}{2}\right) \quad \text{for all } |\lambda| < \frac{1}{\alpha} \\ \implies \mathbb{E}\left[\exp\left(\frac{\lambda}{s}(sX - s\mu)\right)\right] &\leq \exp\left(\frac{\nu^2 s^2 \frac{\lambda^2}{s^2} 2}{2}\right) \quad \text{for all } \left|\frac{\lambda}{s}\right| < \frac{1}{s\alpha} \\ \xrightarrow{\lambda' = \frac{\lambda}{s}} \mathbb{E}[\exp(\lambda'(X' - \mu'))] &\leq \exp\left(\frac{\nu^2 s^2 \lambda'^2}{2}\right) \quad \text{for all } |\lambda'| < \frac{1}{s\alpha} \end{aligned} \quad (10)$$

Defining $\alpha' = s\alpha$ and $\nu' = s\nu$ we recover that $X' \sim SE(s\nu, s\alpha)$. □

Proposition 8. *If the random variables X_i for $i \in [1 - N]$ for $N \in \mathbb{N}^+$ are all sub-exponential with parameters (ν_i, α_i) and independent, then $\sum_{i=1}^N X_i$ is sub-exponential with parameters $(\sqrt{\sum_{i=1}^N \nu_i^2}, \max_i \alpha_i)$.*

Proof. The proof is a simplification of the discussion prior to equation 2.18 in Wainwright (2019).

Proposition 9. *For a random variable $X \sim SE(\nu, \alpha)$, the following concentration inequality holds:*

$$\Pr(|X - \mu| \geq t) \leq 2 \exp\left(-\min\left(\frac{t^2}{2\nu^2}, \frac{t}{2\alpha}\right)\right)$$

Proof. The proof directly follows from applying a scalar multiplication to the result derived in Equation 2.18 in Wainwright, 2019.

Corollary 10. *For a random variable $X \sim SE(\nu, \alpha)$ the following inequality holds with probability at least $1 - \delta$:*

$$|X - \mu| < \max\left(\nu \sqrt{2 \log \frac{2}{\delta}}, 2\alpha \log \frac{2}{\delta}\right)$$

B.2 Pseudo-NTK converges to eNTK as the final layer's width grows

In this subsection, we present a formal proof for Theorem 1. For simplicity and better readability of the equations, we drop the L subscript from θ_L .

Proof. Define $D(x_1, x_2) = \frac{1}{\sqrt{w}} \hat{\Theta}_f(x_1, x_2) \otimes I_O - \frac{1}{\sqrt{w}} \Theta_f(x_1, x_2)$. Expanding the pNTK and eNTK using (9), we get:

$$\begin{aligned} \Theta_f(x_1, x_2)_{ij} &= \theta_i \Theta_g(x_1, x_2) \theta_j^\top + \mathcal{I}(i=j) g(x_1)^\top g(x_2) \\ &= \sum_{a=1}^w \sum_{b=1}^w \theta_{ia} \theta_{jb} \Theta_g(x_1, x_2)_{ab} + \mathcal{I}(i=j) g(x_1)^\top g(x_2) \\ &= \frac{1}{w} \sum_{a=1}^w \sum_{b=1}^w z_{ia} z_{jb} \Theta_g(x_1, x_2)_{ab} + \mathcal{I}(i=j) g(x_1)^\top g(x_2) \end{aligned} \quad (11)$$

and

$$\begin{aligned} \hat{\Theta}_f(x_1, x_2) &= \frac{1}{O} \sum_{c=1}^O \sum_{d=1}^O \Theta_f(x_1, x_2)_{cd} + g(x_1)^\top g(x_2) \\ &= \frac{1}{Ow} \sum_{c=1}^O \sum_{d=1}^O \sum_{a=1}^w \sum_{b=1}^w z_{ca} z_{db} \Theta_g(x_1, x_2)_{ab} + g(x_1)^\top g(x_2) \end{aligned} \quad (12)$$

where \mathcal{I} denotes the indicator function. Thus, $D(x_1, x_2)$ has ij 'th element

$$D(x_1, x_2)_{ij} = \frac{1}{w\sqrt{w}} \begin{cases} \sum_{a=1}^w \sum_{b=1}^w z_{ia} z_{ib} \Theta_g(x_1, x_2)_{ab} - \frac{1}{O} \sum_{c=1}^O \sum_{d=1}^O \sum_{a=1}^w \sum_{b=1}^w z_{ca} z_{db} \Theta_g(x_1, x_2)_{ab} & \text{if } i = j \\ \sum_{a=1}^w \sum_{b=1}^w z_{ia} z_{jb} \Theta_g(x_1, x_2)_{ab} & \text{if } i \neq j. \end{cases}$$

We would like to first find individual bounds for $D(x_1, x_2)_{ii}$ and $D(x_1, x_2)_{ij}$ and then bound the corresponding Frobenius norm of $D(x_1, x_2)$. First, notice that as $W_{i,j} \sim \mathcal{N}(0, \frac{\sigma_L}{w} \omega_{i,j})$, briefly assuming $\sigma_L = 1$ (scaling this parameter doesn't change the order of convergence rate but accordingly scales the parameters (ν, α) of the sub-exponential distribution of interest as we will see later) we substituted θ_{ij} with $\frac{1}{w}$. We can further simplify $D(x_1, x_2)_{ij}$ as

$$D(x_1, x_2)_{ij} = \frac{1}{w\sqrt{w}} \sum_{a=1}^w \sum_{b=1}^w \Theta_g(x_1, x_2)_{ab} \begin{cases} z_{ia} z_{ib} - \frac{1}{O} \sum_{c=1}^O \sum_{d=1}^O z_{ca} z_{db} & \text{if } i = j \\ z_{ia} z_{jb} & \text{if } i \neq j \end{cases}. \quad (13)$$

Now, note that as the product of two independent standard Gaussian random variables $\beta = z_1 z_2$, as the product of two sub-gaussian distributions, is a zero-mean sub-exponential distribution. However, not all products of the form $z_{ia} z_{jb}$ used above are independent, and we need to carefully investigate the interactions. Assuming $\alpha = \|\Theta_g(x_1, x_2)\|_\infty$, we can write

$$\begin{aligned} D(x_1, x_2)_{ii} &\leq \frac{\alpha}{w\sqrt{w}} \left[\underbrace{\sum_{a=1}^w \left(z_{ia}^2 - \frac{1}{O} \sum_{c=1}^O z_{ca}^2 \right)}_{D_1(x_1, x_2)_{ii}} - \underbrace{\frac{1}{O} \sum_{c=1}^O \sum_{d=1, d \neq c}^O z_{ca} z_{da}}_{D_2(x_1, x_2)_{ii}} \right. \\ &\quad \left. + \underbrace{\sum_{a=1}^w \sum_{b=1, b \neq a}^w z_{ia} z_{ib}}_{D_3(x_1, x_2)_{ii}} - \underbrace{\frac{1}{O} \sum_{a=1}^w \sum_{b=1, b \neq a}^w \sum_{c=1}^O \sum_{d=1}^O z_{ca} z_{db}}_{D_4(x_1, x_2)_{ii}} \right]. \end{aligned}$$

We would like to bound each of $D_k(x_1, x_2)_{ii}$ for $k \in \{1, 2, 3, 4\}$ and then find a bound for the diagonal elements using the combination of them. Starting with $D_1(x_1, x_2)_{ii}$:

$$\begin{aligned}
D_1(x_1, x_2)_{ii} &\leq \frac{\alpha}{w\sqrt{w}} \sum_{a=1}^w \left(z_{ia}^2 - \frac{1}{O} \sum_{c=1}^O z_{ca}^2 \right) \\
&= \frac{\alpha}{w\sqrt{w}} \sum_{a=1}^w \left(z_{ia}^2 - \frac{1}{O} z_{ia}^2 - \frac{1}{O} \sum_{c=1, c \neq i}^O z_{ca}^2 \right) \\
&\sim \frac{\alpha}{w\sqrt{w}} \sum_{a=1}^w \left(SE \left(\frac{2(O-1)}{O}, \frac{4(O-1)}{O} \right) - SE \left(\sqrt{\frac{(O-1)^2}{O^2}}, \frac{4}{O} \right) \right) \quad (14) \\
&= \frac{\alpha}{w\sqrt{w}} \sum_{a=1}^w SE \left(\sqrt{\frac{4(O-1)^2}{O^2} + \frac{4(O-1)}{O^2}}, \max \left(\frac{4(O-1)}{O}, \frac{4}{O} \right) \right) \\
&= \frac{2\alpha}{w} SE \left(\sqrt{1 - \frac{1}{O}}, \frac{1}{\sqrt{w}} \left(1 - \frac{1}{O} \right) \right)
\end{aligned}$$

Thus, using Corollary 10, we can claim

$$|D_1(x_1, x_2)_{ii}| < \frac{2\alpha}{w} \sqrt{2 \left(1 - \frac{1}{O} \right) \log \frac{8}{\delta}} \quad (15)$$

with probability at least $1 - \delta/4$.

For the other terms, we can simply the analysis through noting that they are all a form of weighted summation of independent sub-exponential random variables of the same distribution. For such a summation with a weight of a and b summation terms, we have

$$X = a \sum_{i=1}^b z_i z'_i \sim a \sum_{i=1}^b SE(\sqrt{2}, \sqrt{2}) = a SE(\sqrt{2b}, \sqrt{2}). \quad (16)$$

Thus, applying Corollary 10, we get that

$$|X| < 2a \max \left(\sqrt{b \log \frac{8}{\delta}}, \sqrt{2} \log \frac{8}{\delta} \right) \quad (17)$$

with probability at least $1 - \delta/4$. Accordingly we can claim

$$|D_2(x_1, x_2)_{ii}| < \frac{2\alpha}{w\sqrt{w}} \max \left(\sqrt{\left(1 - \frac{1}{O^2} \right) \log \frac{8}{\delta}}, \sqrt{2} \log \frac{8}{\delta} \right), \quad (18)$$

$$|D_3(x_1, x_2)_{ii}| < \frac{2\alpha}{\sqrt{w}} \max \left(\sqrt{\left(1 - \frac{1}{w^2} \right) \log \frac{8}{\delta}}, \sqrt{2} \log \frac{8}{\delta} \right), \quad (19)$$

$$|D_4(x_1, x_2)_{ii}| < \frac{2\alpha}{\sqrt{w}} \max \left(\sqrt{\left(1 - \frac{1}{O^2} - \frac{1}{w^2} + \frac{1}{O^2 w^2} \right) \log \frac{8}{\delta}}, \sqrt{2} \log \frac{8}{\delta} \right), \quad (20)$$

all independently and with probability at least $1 - \delta/4$. Moreover, one can easily see that $D(x_1, x_2)_{ij}$ for $i \neq j$ follows the same inequality (19) as $D_3(x_1, x_2)_{ii}$. Thus, loosening the off-diagonal terms for simplicity, applying a union bound on the previous three inequalities yields

$$|D(x_1, x_2)_{ij}| < \frac{8\alpha}{\sqrt{w}} \max \left(\sqrt{\log \frac{8}{\delta}}, \sqrt{2} \log \frac{8}{\delta} \right) \quad (21)$$

with probability at least $1 - \delta$.

Finally, as $\|D(x_1, x_2)\|_F = \sqrt{\sum_{i,j} D(x_1, x_2)_{ij}^2}$, if each entry's absolute value is less than $t > 0$ then the Frobenius norm is less than tO . Thus we can combine a bound on each of the O^2 entries to see that

$$\Pr \left(\|D(x_1, x_2)\|_F \leq \frac{8O\alpha}{\sqrt{w}} \max \left(\sqrt{\log \frac{8O^2}{\delta}}, \sqrt{2} \log \frac{8O^2}{\delta} \right) \right) \geq 1 - \delta \quad (22)$$

as desired. \square

B.3 Pseudo-NTK's maximum eigenvalue converges to eNTK's maximum eigenvalue as width grows

In this subsection, we present a formal proof for Theorem 5.

Proof. Note that, as both pNTK and eNTK are symmetric PSD matrices, their maximum eigenvalues are equal to their spectral norm. Furthermore, the spectral norm of a matrix is upper-bounded by its Frobenius norm. Now, note that according to the triangle inequality, we have

$$\begin{aligned} \left\| \frac{1}{\sqrt{w}} \Theta_f(x_1, x_2) \right\| &= \left\| \frac{1}{\sqrt{w}} \hat{\Theta}_f(x_1, x_2) \otimes I_O + \left(\frac{1}{\sqrt{w}} \Theta_f(x_1, x_2) - \frac{1}{\sqrt{w}} \hat{\Theta}_f(x_1, x_2) \otimes I_O \right) \right\| \\ &\leq \left\| \frac{1}{\sqrt{w}} \hat{\Theta}_f(x_1, x_2) \otimes I_O \right\| + \left\| \frac{1}{\sqrt{w}} \Theta_f(x_1, x_2) - \frac{1}{\sqrt{w}} \hat{\Theta}_f(x_1, x_2) \otimes I_O \right\| \end{aligned} \quad (23)$$

Thus

$$\left\| \frac{1}{\sqrt{w}} \Theta_f(x_1, x_2) \right\| - \left\| \frac{1}{\sqrt{w}} \hat{\Theta}_f(x_1, x_2) \otimes I_O \right\| \leq \left\| \frac{1}{\sqrt{w}} \Theta_f(x_1, x_2) - \frac{1}{\sqrt{w}} \hat{\Theta}_f(x_1, x_2) \otimes I_O \right\|. \quad (24)$$

which according to (22) together with the fact that for any matrix A , $\lambda_{\max}(A \otimes I) = \lambda_{\max}(A)$ implies that with probability at least $1 - \delta$

$$\left| \lambda_{\max} \left(\frac{1}{\sqrt{w}} \Theta_f(x_1, x_2) \right) - \lambda_{\max} \left(\frac{1}{\sqrt{w}} \hat{\Theta}_f(x_1, x_2) \right) \right| \leq \frac{8O\alpha}{\sqrt{w}} \max \left(\sqrt{\log \frac{8O^2}{\delta}}, \sqrt{2} \log \frac{8O^2}{\delta} \right) \quad (25)$$

\square

as desired.

B.4 Kernel regression using pNTK vs Kernel regression using eNTK

In this subsection we provide a formal proof for Theorem 6.

Proof. We start by proving a simpler version of a theorem, and then show a correspondence that expands the result of the simpler proof to the original Theorem. Assuming $|\mathcal{X}| = |\mathcal{Y}| = N$ (training data), we define

$$h(x) = \Theta_f(x_1, \mathcal{X}) \Theta_f(\mathcal{X}, \mathcal{X})^{-1} \mathcal{Y} \text{ and } \hat{h}(x) = \left(\hat{\Theta}_f(x_1, \mathcal{X}) \otimes I_O \right) \left(\hat{\Theta}_f(\mathcal{X}, \mathcal{X}) \otimes I_O \right)^{-1} \mathcal{Y}. \quad (26)$$

Note that as the result of kernel regression (without any regularization) does not change with scaling the kernel with a fixed scalar, we can use a weighted version kernels mentioned in the previous equation without loss of generality. Accordingly, we define

$$\alpha = \left(\frac{1}{\sqrt{w}} \Theta_f(\mathcal{X}, \mathcal{X}) \right)^{-1} \mathcal{Y} \text{ and } \hat{\alpha} = \left(\frac{1}{\sqrt{w}} \hat{\Theta}_f(\mathcal{X}, \mathcal{X}) \otimes I_O \right)^{-1} \mathcal{Y}. \quad (27)$$

Using the fact that $\hat{M}^{-1} - M^{-1} = -\hat{M}^{-1}(\hat{M} - M)M^{-1}$ and $(A \otimes I)^{-1} = A^{-1} \otimes I$ we can show that

$$\hat{\alpha} - \alpha = -\hat{\Theta}_f(\mathcal{X}, \mathcal{X})^{-1} \otimes I_O \left(\frac{1}{\sqrt{w}} \hat{\Theta}_f(\mathcal{X}, \mathcal{X}) \otimes I_O - \frac{1}{\sqrt{w}} \Theta_f(\mathcal{X}, \mathcal{X}) \right)^{-1} \Theta_f(x_1, x_2) \mathcal{Y} \quad (28)$$

Assume $\lambda = \min(\lambda_{\min}(\Theta_f(\mathcal{X}, \mathcal{X})), \lambda_{\min}(\hat{\Theta}_f(\mathcal{X}, \mathcal{X})))$. Then

$$\|\hat{\alpha} - \alpha\| \leq \frac{1}{\lambda^2} \left\| \frac{1}{\sqrt{w}} \hat{\Theta}_f(\mathcal{X}, \mathcal{X}) \otimes I_O - \frac{1}{\sqrt{w}} \Theta_f(\mathcal{X}, \mathcal{X}) \right\| \|\mathcal{Y}\| \quad (29)$$

Plugging into the formula for kernel regression, we get that

$$\begin{aligned} \hat{h}(x) - h(x) &= \left(\frac{1}{\sqrt{w}} \hat{\Theta}_f(x, \mathcal{X}) \otimes I_O \right) \hat{\alpha} - \frac{1}{\sqrt{w}} \Theta_f(x, \mathcal{X}) \alpha \\ &= \left(\frac{1}{\sqrt{w}} \hat{\Theta}_f(x, \mathcal{X}) \otimes I_O - \frac{1}{\sqrt{w}} \Theta_f(x, \mathcal{X}) \right) \hat{\alpha} + \frac{1}{\sqrt{w}} \Theta_f(x, \mathcal{X}) (\hat{\alpha} - \alpha) \end{aligned} \quad (30)$$

Thus

$$\begin{aligned} \|\hat{h}(x) - h(x)\| &\leq \left\| \frac{1}{\sqrt{w}} \hat{\Theta}_f(x, \mathcal{X}) \otimes I_O - \frac{1}{\sqrt{w}} \Theta_f(x, \mathcal{X}) \right\| \|\hat{\alpha}\| + \left\| \frac{1}{\sqrt{w}} \Theta_f(x, \mathcal{X}) \right\| \|\hat{\alpha} - \alpha\| \\ &\leq \frac{1}{\lambda} \left\| \frac{1}{\sqrt{w}} \hat{\Theta}_f(x, \mathcal{X}) \otimes I_O - \frac{1}{\sqrt{w}} \Theta_f(x, \mathcal{X}) \right\| \|\mathcal{Y}\| \\ &\quad + \frac{1}{\lambda^2} \left\| \frac{1}{\sqrt{w}} \Theta_f(x, \mathcal{X}) \right\| \left\| \frac{1}{\sqrt{w}} \hat{\Theta}_f(\mathcal{X}, \mathcal{X}) \otimes I_O - \frac{1}{\sqrt{w}} \Theta_f(\mathcal{X}, \mathcal{X}) \right\| \|\mathcal{Y}\|. \end{aligned} \quad (31)$$

Now, note that as for a block matrix A of A_{ij} blocks we have that $\|A\| \leq \sum_{i,j} \|A_{ij}\|$ it follows that for any matrix valued kernel K

$$\|K(\mathcal{X}, \mathcal{X})\| \leq \sum_{x_1, x_2 \in \mathcal{X}} \|K(x_1, x_2)\|. \quad (32)$$

Using this fact, we can rewrite the bound as

$$\begin{aligned} \|\hat{h}(x) - h(x)\| &\leq \frac{N}{\lambda} \left\| \frac{1}{\sqrt{w}} \hat{\Theta}_f(x, x_1^*) \otimes I_O - \frac{1}{\sqrt{w}} \Theta_f(x, x_1^*) \right\| \|\mathcal{Y}\| \\ &\quad + \frac{N^2}{\lambda^2} \left\| \frac{1}{\sqrt{w}} \Theta_f(x, \mathcal{X}) \right\| \left\| \frac{1}{\sqrt{w}} \hat{\Theta}_f(x_2^*, x_3^*) \otimes I_O - \frac{1}{\sqrt{w}} \Theta_f(x_2^*, x_3^*) \right\| \|\mathcal{Y}\| \end{aligned} \quad (33)$$

for some particular $x_1^*, x_2^*, x_3^* \in \mathcal{X}$. Using (22), we can see with probability at least $1 - \delta$ that

$$\|\hat{h}(x) - h(x)\| \leq \frac{8NO\alpha}{\lambda\sqrt{w}} \max \left(\sqrt{\log \frac{8O^2}{\delta}}, \sqrt{2} \log \frac{8O^2}{\delta} \right) \|\mathcal{Y}\| \left(1 + \frac{N}{\lambda} \left\| \frac{1}{\sqrt{w}} \Theta_f(x, \mathcal{X}) \right\| \right). \quad (34)$$

To show the correspondence between $\hat{h}(x)$ and $\hat{f}^{lin}(x)$, as in (6), note that

$$\begin{aligned} \hat{h}(x) &= \left(\hat{\Theta}_f(x, \mathcal{X}) \otimes I_O \right) \left(\hat{\Theta}_f(\mathcal{X}, \mathcal{X})^{-1} \otimes I_O \right) \mathcal{Y} \\ &= \left(\hat{\Theta}_f(x, \mathcal{X}) \hat{\Theta}_f(\mathcal{X}, \mathcal{X})^{-1} \otimes I_O \right) \mathcal{Y} \\ &= \text{vec} \left(I_O \mathcal{Y}_v \hat{\Theta}_f(x, \mathcal{X}) \hat{\Theta}_f(\mathcal{X}, \mathcal{X})^{-1} \right) \end{aligned} \quad (35)$$

where $\mathcal{Y}_v = \text{vec}^{-1}(\mathcal{Y})$ is the result of inverse of the vectorization operation, converting the $NO \times 1$ vector to a $O \times N$ matrix. Thus, $\hat{h}(x) = \hat{\Theta}_f(x, \mathcal{X}) \hat{\Theta}_f(\mathcal{X}, \mathcal{X})^{-1} \mathcal{Y}'$ where \mathcal{Y}' is the $N \times O$ matrix derived from reshaping the $NO \times 1$ vector \mathcal{Y} . The proof is complete. \square

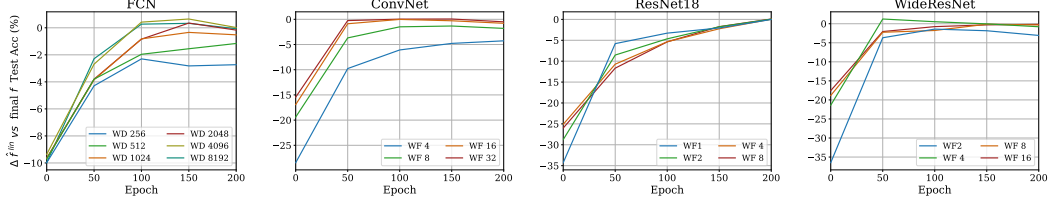


Figure 12: Evaluating the **difference in test accuracy of kernel regression using pNTK as in (6) vs the final model f** throughout SGD training on the full Cifar-10 dataset. How much worse would it be to “give up” on SGD at this point and train \hat{f}^{lin} with the current representation

C More details on kernel Regression using pNTK on full Cifar-10 dataset

In this section we provide another figure comparing the accuracy of $\hat{f}^{lin}(x)$ with parameters derived at epoch $E \in \{0, 50, 100, 150, 200\}$ of training the NN with SGD. On the y-axis, the reported number is $\hat{f}^{lin}(x) - f^*(x)$ where f^* denotes the final model obtained after training f for 200 epochs. As seen in Figure 12 the architecture of the model has a significant impact on how good the linearization predicts the final accuracy of the fully-trained model. However, as proven in Theorem 1 in conjunction with the linearization approximations provided in Lee et al. (2019), as width grows, this approximation becomes more accurate. One unexplored fact regarding this experiment is that fact that linearization with trained parameters significantly outperforms linearization at initialization, which is intuitive but not rigorously investigated yet.